Grain growth in thin films by a discrete model based on pair interactions

Paolo Emilio Di Nunzio*
Centro Sviluppo Materiali S.p.A., Via di Castel Romano 100-102, I-00128 Rome, Italy
(Received 6 January 2003; published 29 September 2003)

A discrete model is presented which predicts the curvature-driven grain growth kinetics and the grain size distribution in polycrystalline thin films. A probabilistic approach based on elementary exchanges of volume between grain pairs and a simple topological description of the system have been used to define the basic structure of the growth rate equations. In addition, the local grain-boundary curvature has been introduced in each contact between nearest neighbors instead of the average curvature adopted in mean-field models. Even in absence of inhibition right-skewed quasistationary grain-size distributions are obtained. The topological features of the polycrystal predicted by the model are compatible with the currently accepted theories and the available experimental data. The results of simulations with a constant inhibition term in the growth equation are also discussed. A comparison with experimental data and models in the literature indicates that the present formulation has a capability in predicting the shape of the grain-size distributions better than previous analytical approaches and comparable with that of numerical algorithms.

DOI: 10.1103/PhysRevB.68.115432 PACS number(s): 07.05.−t

I. INTRODUCTION

Grain growth in two dimensions has been studied since long ago due to the ease in comparing the model predictions with the directly measurable features of real materials and to a well established theoretical and topological background.[1–12] Since the time the classic paper by Hillert[1] appeared, it has been observed that the two-dimensional (2D) self-preserving grain-size distribution (GSD) characterizing the quasistationary regime of coarsening is sharper than that predicted in 3D systems. Much work has been performed to get a deeper insight to the theoretical aspects. Many of the analytical approaches are based on the assumption that the average curvature of the grains, proportional to the reciprocal of their linear size, could be used to evaluate the growth rate. All models generally agree in predicting that the average grain size increases proportionally to the square root of time but they are often not equally accurate in reproducing the experimental GSD. On the other hand, remarkable results have been obtained by Monte Carlo models[2–4,13] that, using elementary rules of the microscopic behavior of grain boundaries, do not suffer from the usual shortcomings of the analytical models based on the average curvature.

It has been argued that the inaccuracies in the prediction of the GSD shape could arise from the excessive simplification of the average curvature hypothesis.[14,15] The major result of the grain growth model presented here is that, although it extends the probabilistic approach by Abbruzzese[16] and Abbruzzese and Lücke,[17] and it is based on the analytical formulation by Hillert, it is characterized by a markedly right-skewed GSD, in agreement with both experiments and numerical models such as Monte Carlo[2–4] and Surface Evolver.[10] This result has been achieved by the explicit consideration of pairwise interactions among grains and by using the *local* boundary curvature of each grain face rather than its average value.

The theory, which predicts the microstructural evolution in single-phase polycrystalline systems, is specific for thin films where the average grain size is comparable with the film thickness and where the grain boundaries are perpendicular to the film surface and go across its whole thickness. To outline the specific merits of the model, a comparison with the same theoretical approach but where the average boundary curvature was used instead of the local curvature is also presented and discussed.

The presence of a crystallographic texture is not considered and the properties of all grain boundaries (mobility and specific energy) are supposed constant throughout the system. The work is principally focused on the prediction of the GSD shape rather than on the aspects related to the coarsening kinetics.

II. THEORY

A. General structure of the model

The grain growth model presented here can be thought of as composed by different submodels, each accounting for a specific aspect. First, the topological features of the polycrystalline thin film have to be specified to permit the calculation of the size-dependent number of nearest neighbors of a grain and the area of each contact surface. A simple geometrical model has been used for this purpose which, although approximate, gives exact predictions of the average polycrystal properties. Then, a growth equation is defined, where the driving force for the process is expressed. Finally, the volume conservation constraint is imposed to calculate the evolution of the GSD. Of course, the mathematical form of the required continuity equation is determined by the approach adopted in the growth model and, in the present case, it reflects the structure of pair interactions. This results in substantial differences with respect to Hillert's model.[1]

The grain-size distribution is defined over a discrete set of equally spaced classes of grain radius R_i, by the number of grains per unit volume in the ith class n_i. Grain boundaries are assumed to be perpendicular to the film surface, thence the linear dimension characterizing the grain size is defined in terms of the radius of the equivalent cylinder as

$$v_i = \pi R_i^2 h, \tag{2.1}$$

where h is the film thickness. In the following sections a detailed description of all the components is given.

B. Topology

The contact area A_{ij} of a common face shared between two grains R_i and R_j is expressed as

$$A_{ij} = \frac{2\pi h}{3} \cdot \frac{R_i R_j}{R_i + R_j}. \tag{2.2}$$

Equation (2.2), symmetrical with respect to the exchange of indices, has been derived by adding the factor $\pi/3$ from Ref. 7 according to a simplified geometrical model based on circular grains. The accuracy in describing the topology of 2D systems can be verified by calculating the number of neighbors in a monodispersed system ($R_i = R_j$) which is given by the ratio between the boundary surface of a grain and the surface of a single contact:

$$\langle m_{2D} \rangle = \frac{2\pi R_i h}{A_{ij}} = 6. \tag{2.3}$$

This result coincides with the theoretical value for a polygonal tessellation of the plane with triple junctions only. On the other hand, as the ratio R_j/R_i approaches zero, A_{ij} tends to $2\pi R_i h/3$ and the number of nearest neighbors of the smallest grains is $m_{\min} = 3$. It has to be noticed that this simple geometrical model does not permit the existence of two-sided grains.

For each size class, the average number of neighbors (grain faces) m_i, is defined as

$$m_i = \frac{2\pi R_i h}{\langle A_i \rangle}, \tag{2.4}$$

where $\langle A_i \rangle$ is the average area of a contact in the ith class. Its evaluation is carried out by averaging the surfaces of single contacts A_{ij}, weighted by their number given by the product between n_i and m_i as follows:

$$\langle A_i \rangle = \sum_{j=1}^{n_c} \frac{n_j m_j}{\sum_{k=1}^{n_c} n_k m_k} A_{ij}, \tag{2.5}$$

where n_c is the number of size classes in the GSD. By substituting in Eq. (2.5) the definition of m_i from Eq. (2.4), one obtains

$$\langle A_i \rangle = \sum_{j=1}^{n_c} \frac{n_j R_j A_{ij} / \langle A_j \rangle}{\sum_{k=1}^{n_c} n_k R_k / \langle A_k \rangle}. \tag{2.6}$$

The set of $\langle A_i \rangle$ is found by iteration and the m_i are then calculated by Eq. (2.4).

C. Kinetics

Grain growth is treated in terms of superposition of elementary exchanges of volume between neighbors, the overall growth or shrinkage of a grain depending on its surrounding. For each contact, the boundary displacement produces a volume change with a rate proportional to the difference between the effective boundary curvature of the pair of facing grains. Assuming that $R_i > R_j$, this can be expressed in a general form as

$$\left.\frac{dv_i}{dt}\right|_j = M\gamma A_{ij}(\kappa_{ji} - \kappa_{ij} - Z) \quad \text{for } |\kappa_{ji} - \kappa_{ij}| \geqslant Z, \tag{2.7a}$$

$$\left.\frac{dv_i}{dt}\right|_j = 0 \qquad \text{for } |\kappa_{ji} - \kappa_{ij}| < Z, \tag{2.7b}$$

where M is the grain boundary mobility, γ the interfacial energy, both constant throughout the system, κ_{ij} is the local boundary curvature, and Z a positive inhibition term, always opposed to the boundary motion and related to the presence of dispersed second phase particles.[4,18,19] Also surface effects[20] or stresses induced by a substrate, generally thicker than the film and with different elastic and thermal properties,[9] can inhibit the grain-boundary motion. The volume balance requires that, for the smaller grain j, the boundary velocity is calculated as

$$\left.\frac{dv_j}{dt}\right|_i = -\left.\frac{dv_i}{dt}\right|_j. \tag{2.8}$$

To evaluate the boundary curvature, the commonly used approximation of taking its average value, irrespective of the neighbors' size, could be adopted. In this case, one obtains

$$\kappa_{ij} \equiv \kappa_i = \frac{1}{R_i}. \tag{2.9}$$

In the present approach, the alternative use of the local grain-boundary curvature is proposed, which, instead, depends on the size of the neighbor sharing a common face with the reference grain. The local curvature of the grain i with respect to the contact with j is calculated according to the general definition[21] as

$$\kappa_{ij} = \left.\frac{dS_i}{dv_i}\right|_j, \tag{2.10}$$

where S_i is the overall boundary surface given by

$$S_i = A_{ij} m_i. \tag{2.11}$$

According to Eq. (2.10) and from Eqs. (2.1) and (2.11) one obtains

$$\kappa_{ij} = \frac{1}{2\pi R_i h}\left(m_i \left.\frac{\partial A_{ij}}{\partial R_i}\right|_{R_i, R_j} + A_{ij} \left.\frac{\partial m_i}{\partial R_i}\right|_{R_i} \right), \tag{2.12}$$

where the derivatives are calculated at the point (R_i, R_j). After simple algebraic manipulations using Eq. (2.2) one obtains

$$\kappa_{ij} = \frac{R_j}{3R_i(R_i + R_j)}\left(\frac{m_i R_j}{(R_i + R_j)} + R_i \left.\frac{\partial m_i}{\partial R_i}\right|_{R_i} \right). \tag{2.13}$$

The overall volume exchange between ith and jth size classes is given by

$$w_{ij}\left.\frac{dv_i}{dt}\right|_j = -w_{ji}\left.\frac{dv_j}{dt}\right|_i, \tag{2.14}$$

where w_{ij} and w_{ji} are the number of contacts per unit volume subjected to the obvious symmetry condition $w_{ij}=w_{ji}$. The quantity w_{ij} is defined as the product between the number of faces per unit volume m_v and the contact probability between i and j, p_{ij}:

$$w_{ij}=m_v p_{ij} \tag{2.15}$$

with

$$m_v=\frac{1}{2}\sum_{i=1}^{n_c} n_i m_i. \tag{2.16}$$

The probability p_{ij} is calculated by means of elementary principles assuming that any contact i-j results from independent events represented by the occurrence of a face in each size class as

$$p_{ij}=\frac{n_i m_i}{\Sigma_{k=1}^{n_c} n_k m_k}\cdot\frac{n_j m_j}{\Sigma_{k=1}^{n_c} n_k m_k}, \tag{2.17}$$

so that the following expression for w_{ij} results:

$$w_{ij}=\frac{n_i m_i n_j m_j}{2\Sigma_{k=1}^{n_c} n_k m_k}. \tag{2.18}$$

Finally, the average number of faces per grain in the system is calculated as

$$\langle m\rangle=\frac{2m_v}{N_v}=\frac{1}{N_v}\sum_{i=1}^{n_c} n_i m_i, \tag{2.19}$$

where N_v is the number of grains per volume unit given by

$$N_v=\sum_{i=1}^{n_c} n_i. \tag{2.20}$$

It has to be noted that Eq. (2.9) results from Eq. (2.10) when the overall boundary surface in Eq. (2.11) is written as $S_i=\langle A_i\rangle\, m_i$ using the definition of m_i from Eq. (2.4).

D. Continuity equation

The continuity equation used in Hillert's model[1] cannot be applied to the present discrete formulation. For calculating the evolution of the GSD shape, the conditions of volume balance and conservation of grain number must be imposed by the following integrodifferential equation for the volume distribution $n(v)$ in the continuous domain:

$$\frac{\partial n(v)}{\partial t}=\int_0^v \frac{\partial}{\partial v}\left(w(v,\tilde{v})\left.\frac{dv}{dt}\right|_{\tilde{v}}\right)d\tilde{v} - \int_v^\infty \frac{\partial}{\partial \tilde{v}}\left(w(\tilde{v},v)\left.\frac{d\tilde{v}}{dt}\right|_{v}\right)d\tilde{v}, \tag{2.21}$$

where $w(v,\tilde{v})$ is the continuous equivalent of the discrete w_{ij}. The two terms in the right-hand side represent the positive contributions from contacts between grains with $\tilde{v}<v$ and the withdrawal from those with $\tilde{v}>v$, respectively. Details of this derivation can be found in Ref. 14.

Generally speaking, the hypothesis underlying the strategy for evaluating the change in number of grains of size classes is that each interacting pair is independent on the others. Thus the overall balance is obtained by simply adding all the possible elementary contributions. This implies that, focusing on a single grain class, all the possible surroundings (in terms of a distribution of sizes of the nearest neighbors), are taken into account in a statistical sense.

For practical computation purposes, the main features of the discrete algorithm can be summarized as follows. The overall volume exchange per unit volume between classes i and j in the time interval Δt is

$$\Delta V_{ij}=w_{ij}\left.\frac{dv_i}{dt}\right|_j \Delta t=-\Delta V_{ji}. \tag{2.22}$$

Assuming as before that $R_i>R_j$, the grain i always grows and ΔV_{ij} is always positive. Grains changing their volume are supposed to move from the original ith size class, to the kth. In order to allow for the total volume and number of grains to be conserved, an auxiliary class adjacent to the destination class is introduced. For growing grains this will be the $(k+1)$th (with $k\geqslant i$), whereas for shrinking grains it will be the $(k-1)$th (with $1<k\leqslant j$). In a time step, the volume increase ΔV_{ij} of the w_{ij} interacting grains in the ith class must be partitioned between the classes k and $k\pm1$.

The index of the destination class is calculated through the final volume $v_k^\star$ given by

$$v_k^\star=v_i+\frac{\Delta V_{ij}}{w_{ij}}\ \text{(growing side)}, \tag{2.23a}$$

$$v_k^\star=v_i-\frac{\Delta V_{ij}}{w_{ij}}\ \text{(shrinking side)} \tag{2.23b}$$

from which the corresponding radius $R_k^\star$ is

$$R_k^\star=\left(\frac{v_k^\star}{\pi h}\right)^{1/2}. \tag{2.24}$$

Finally, the class index is given by

$$k=\left[\frac{R_k^\star}{\Delta R}\right]\ \text{(growing side)}, \tag{2.25a}$$

$$k=\left[\frac{R_k^\star}{\Delta R}\right]+1\ \text{(shrinking side)}, \tag{2.25b}$$

where the square brackets indicate that the integer part has to be taken.

The change of the number of elements in the size classes compatible with the transferred volume is evaluated by solving the mass balance condition together with the conservation of the total number of grains. It results in the following relationships:

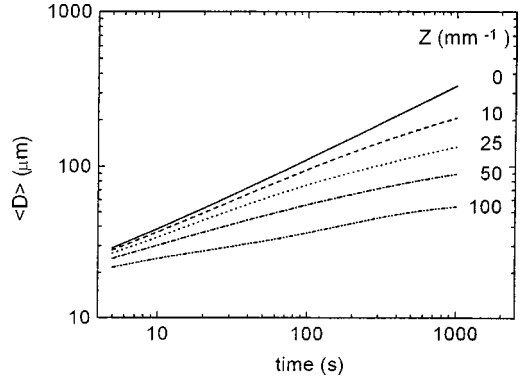

FIG. 1. Growth kinetics of the average grain diameter $\langle D \rangle$ as a function of the inhibition level.

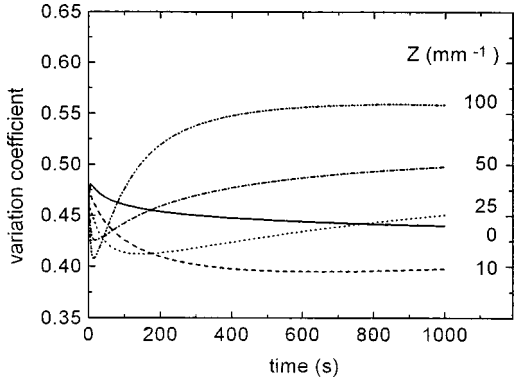

FIG. 2. Evolution of the ratio between the standard deviation of the grain-size distribution and the average size as a function of the inhibition level.

$$\Delta n_k = \pm \frac{w_{ij}(v_{k\pm1} - v_i) - \Delta V_{ij}}{v_{k\pm1} - v_k}, \tag{2.26a}$$

$$\Delta n_{k\pm1} = w_{ij} - \Delta n_k, \tag{2.26b}$$

where the plus and minus signs refer to the growing and shrinking side, respectively. The updated GSD is then obtained as

$$n_i(t+\Delta t) = n_i(t) - w_{ij}, \tag{2.27a}$$

$$n_k(t+\Delta t) = n_k(t) + \Delta n_k, \tag{2.27b}$$

$$n_{k\pm1}(t+\Delta t) = n_{k\pm1}(t) + \Delta n_{k\pm1}. \tag{2.27c}$$

When the first size class is involved ($k=1$), the number of grains is not conserved to permit their complete shrinkage. The only relevant quantity Δn_1 is therefore directly obtained as

$$\Delta n_1 = n_{i1} - \frac{\Delta V_{i1}}{v_1} \tag{2.28}$$

being the volume of the 0th class $v_0 = 0$.

Equations (2.27) are also used to control the integration time step Δt. The latter is chosen as the largest value which produces a non-negative number of elements in the size classes.

III. CALCULATION RESULTS

Simulations have been carried out using the local grain-boundary curvature from Eq. (2.12) on an ideal system with $M = 9 \times 10^{-11}$ m^4 J^{-1} s^{-1} and $\gamma = 0.5$ J m^{-2}. A constant inhibition ranging from 0 to 100 mm^{-1} has been also assumed without specifying whether it depends on boundary pinning by second phases, surface grooving, strain induced by a substrate, or other causes. An initial Gaussian GSD with 5 μm average size, 2.5 μm standard deviation, and a class width $\Delta R = 2$ μm has been used in all cases. A coarsening time of 1000 s has been considered.

Figure 1 shows the plot of the average grain size versus time in double logarithmic scale. The evolution of the variation coefficient $k_{GSD} = \sigma_D / \langle R \rangle$, the ratio between the standard deviation of the GSD and the average size, is reported in Fig. 2. Indicative values of k_{GSD}, normalized skewness coefficient (a_3), growth rate exponent $[d \ln(\langle R \rangle)/d \ln(t)]$ and $\langle m \rangle$ are reported in Table I.

For normal grain growth without inhibition, the quasistationary GSD is shown in Fig. 3 as a function of the reduced size ρ ($\rho = R/\langle R \rangle$) together with the asymptotic analytical 2D solution by Hillert[1] ($k_{GSD} = 0.33$) and that from Marthinsen *et al.*[10] obtained in the numerical simulations by the Surface Evolver program.

The distribution of the total number of faces ($n_i \cdot m_i$) versus the average number of sides (m_i) associated with the

TABLE I. Summary of the relevant kinetic and topological parameters calculated as a function of the inhibition level after 1000 s of simulation time.

Z (mm^{-1})	k_{GSD}	a_3	$\frac{d \ln(\langle R \rangle)}{d \ln(t)}$	$\langle m \rangle$
0[a]	0.440	0.201	0.47	6.00
10[a]	0.398	1.137	0.31	6.00
25[a]	0.451	2.164	0.23	6.00
50[a]	0.498	2.963	0.18	6.00
100[a]	0.558	4.241	0.11	6.00
0[b]	0.382	0.038	0.47	6.00

[a]Local grain-boundary curvature.

[b]Average grain-boundary curvature.

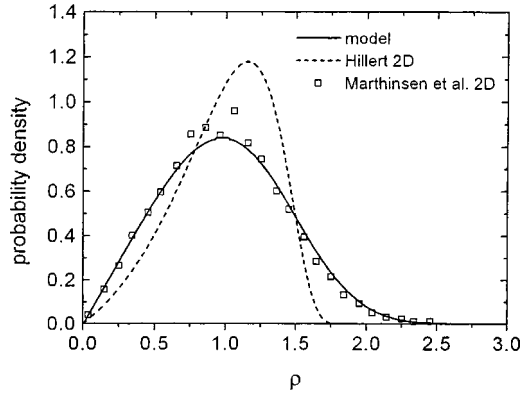

FIG. 3. Comparison among the calculated quasistationary GSD (solid line), the asymptotic solution of the 2D model by Hillert (dashed line), and the distribution obtained by averaging the results of numerical calculations by the Surface Evolver program (squares).

uninhibited system in the quasistationary regime is shown in Fig. 4. It has been also found to be independent of Z within the numerical roundoff errors. Maximum and mean value are both about 6.27. It has to be observed that the latter is given by

$$\langle m_n \rangle = \sum_{i=1}^{n_c} n_i m_i^2 \Big/ \sum_{i=1}^{n_c} n_i m_i . \tag{3.1}$$

The quantity $\langle m_n \rangle$ may be defined as the number of faces of the ''average grain'' and clearly $\langle m_n \rangle \neq \langle m \rangle$.

The average number of faces per class versus the reduced size is shown in Fig. 5. Data are very well approximated by the following linear fit:

$$m(\rho) = 3.13 + 2.85\rho. \tag{3.2}$$

No deviations are found when inhibition is varied.

Finally, the reduced shape of the GSD at different inhibition levels after 1000 s of simulation is reported in Fig. 6. In order to quantify the effect of the boundary curvature approach, similar simulation conditions have been used to calculate the grain growth kinetics without inhibition adopting the average boundary curvature from Eq. (2.9) instead of the local one. The results are reported in the last row of Table I.

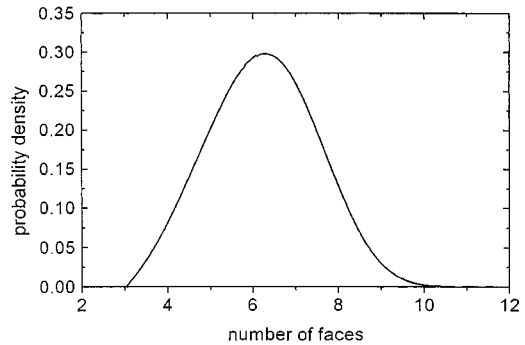

FIG. 4. Distribution of the occurrence of grain faces $(n_i \cdot m_i)$ as a function of the average number of faces m_i.

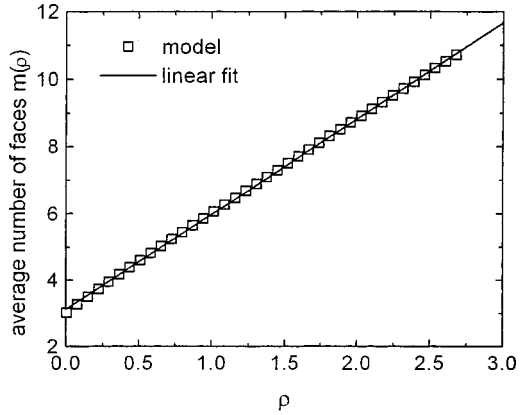

FIG. 5. Relationship between the average number of faces per size class and the reduced grain size.

In the present conditions, the average number of faces per class has shown a dependence on the reduced radius very similar to that in Eq. (3.2).

IV. DISCUSSION

A. General remarks

It has to be noted that the film thickness, inserted explicitly in the theory for the sake of clarity, algebraically cancels out in the growth Eq. (2.7) according to the definition of grain volume [Eq. (2.1)] and contact area [Eq. (2.2)]. Therefore, as expected, it does not influence the system kinetics. Instead, the film thickness directly enters the inhibition term, for example, when grain-boundary grooves are formed at the film surface.[20]

The proposed model predicts a growth exponent for uninhibited coarsening of 0.47, very close to the theoretical value of $\frac{1}{2}$ for surface-driven growth processes. Similar to the 3D case, the growth exponent is reduced as the inhibition is increased and, after an initial transient, the system evolves towards a quasistationary state with a constant value of the variation coefficient k_{GSD} corresponding to a self-preserving shape of the GSD. In the meantime, with increasing the inhibition, the distribution becomes sharper and subsequently broadens while the skewness increases continuously.

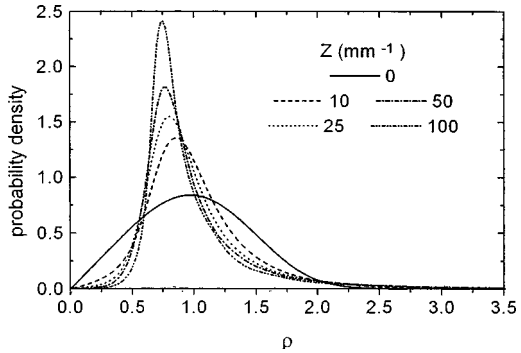

FIG. 6. Quasistationary grain-size distributions after 1000-s simulation with different inhibition levels.

The topological features related to Eq. (3.2) are in agreement with the behavior predicted by some 2D theories from the literature. As a matter of fact, the relationship

$$m(\rho)=3+3\rho \tag{4.1}$$

is reported by different authors.[8,22,23]

Although in Eq. (3.2) the intercept is not exactly equal to 3, the average number of faces predicted for grains with the average size $\rho=1$ is very close to the expected value of 6 representing an actual topological constraint for the system. Concerning the size distribution in absence of inhibition, it is clear from Fig. 3 that the model predicts a right-skewed GSD, substantially different from that of the 2D Hillert's model, with a tail extending beyond the cutoff value $\rho=2$ predicted by Ref. 1. In addition, it closely resembles that proposed in Ref. 10, obtained by numerical simulation with the Surface Evolver program on a 2D region limited by cyclic boundary conditions.

Due to the discrete nature of the present model, it is not possible to deduce an analytical expression for the asymptotic GSD. For comparison, the same model where the average grain-boundary curvature is used instead of the local curvature produces a similar kinetic behavior but a sharper and more symmetrical GSD similar to that by Hillert even if slightly broader (Table I).

B. Topological aspects: The von Neumann–Mullins relationship

Various studies on the topological correlations have been carried out for 2D grain structures.[5,7,8,10,24–28] In the present section, the effect of the grain-boundary curvature on the von Neumann–Mullins (vNM) relationship[7,10,29–31] is examined by comparing the average curvature model, where $\kappa_i=1/R_i$, Eq. (2.9), with that for the local curvature κ_{ij} given by Eq. (2.12). The vNM equation relates the growth rate of the area of a m-sided grain ($\Sigma_m=\pi R_m^2$) to the number of faces according to

$$\frac{d\Sigma_m}{dt}=\frac{\pi}{3}M\gamma(m-6). \tag{4.2}$$

The fundamental assumptions for this relationship to hold are:

(i) all grain boundaries possess equal mobility and surface tension irrespective of their misorientation and crystallographic orientation of the boundaries;
(ii) the mobility of a grain boundary is independent of its velocity;
(iii) triple junctions do not affect grain-boundary motion and therefore angles at triple junctions are in equilibrium.

From the assumptions (i) and (iii), all the angles at the junctions are expected to be equal to 120°. Conversely, lack of equilibrium at triple points implies a deviation from the theoretical value.[32,33]

From Eq. (2.1), the surface area of a grain in the size class i Σ_i, is related to the grain volume through $v_i=\Sigma_i\cdot h$. The average area growth rate *per grain* is deduced from Eq. (2.22) by summing up the contributions from all the possible contacts:

$$\left\langle\frac{d\Sigma_i}{dt}\right\rangle=\frac{1}{hn_i}\sum_{j=1}^{n_c}w_{ij}\left.\frac{dv_i}{dt}\right|_j. \tag{4.3}$$

By substituting in Eq. (4.3) Eqs. (2.7) and (2.18), the following expression is obtained:

$$\left\langle\frac{d\Sigma_i}{dt}\right\rangle=\frac{\pi}{3}M\gamma\frac{m_iR_i}{\sum_{k=1}^{n_c}n_km_k}\sum_{j=1}^{n_c}\frac{n_jm_jR_j}{R_i+R_j}(\kappa_{ji}-\kappa_{ij}), \tag{4.4}$$

which has a similar structure as Eq. (4.2).

In order to facilitate the comparison, it is convenient to deal with a normalized form of Eq. (4.4). Therefore from the ratio between the size-dependent growth rate

$$\frac{d\langle\Sigma\rangle}{dt}=2\pi\langle R\rangle\frac{d\langle R\rangle}{dt}, \tag{4.5}$$

and the growth rate of the average grain $d\langle\Sigma\rangle/dt$, derived from the kinetic calculation according to Ref. 10, the dimensionless area growth rate ν_A is calculated as

$$\nu_A(i)=\left\langle\frac{d\Sigma_i}{dt}\right\rangle\Big/\frac{d\langle\Sigma\rangle}{dt}. \tag{4.6}$$

The plot of $\nu_A(\rho)$ versus the average number of faces $m(\rho)-6$ is shown in Fig. 7 for both the mean curvature and the local curvature models. It can be immediately observed that the average curvature model gives an exact linear relationship whereas the local curvature model exhibits a certain deviation only approximating the expected behavior. On one hand, the first result indicates that the structure of the model is formally correct, otherwise the vNM relationship would have not been recovered. On the other hand, it is necessary to analyze the reason for the approximate behavior of the local curvature model. From the conditions for the validity of the vNM relationship shown above, the result here obtained can be interpreted in terms of a deviation from the equilibrium

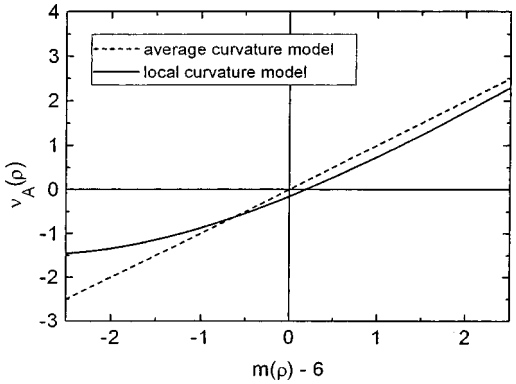

FIG. 7. Von Neumann–Mullins plot showing the comparison between the present model with local boundary curvature (solid curve) and the same model with the average boundary curvature (dashed line).

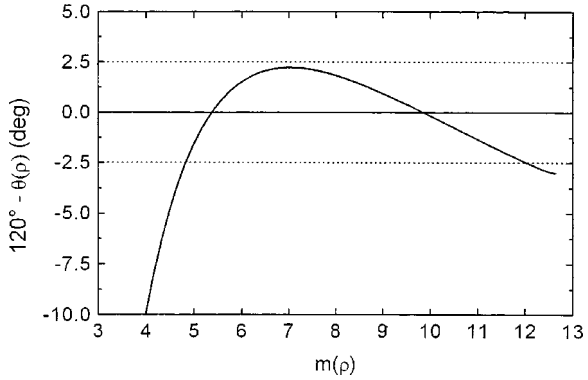

FIG. 8. Displacement of the average internal angle of triple junctions from the equilibrium value 120°, as a function of the topological grain class in the present model with local boundary curvature.

angles at the triple junctions induced by the local curvature only, and not from the average curvature.

Starting from the observation that in both cases the average number of faces per grain in the system is exactly $\langle m \rangle = 6$ (see Table I), which implies that the *average* angle at triple junctions is 120°, it is possible to calculate the variation of the average junction angle as a function of the grain size when the local curvature is used. Thus it is necessary to rewrite Eqs. (4.4) and (4.6) in a form similar to Eq. (4.2) introducing a factor $\pi/3$ to convert the result in angular quantities. Due to the normalization (4.6), the slope of the straight line obtained by the average curvature model in Fig. 7 is equal to unity.

With reference to the derivation of Eq. (4.2) by Mullins,[30] for a circuit around a grain having an average number of sides equal to $m(\rho)$, one can write the vNM relationship as

$$\nu_A^\star(\rho) = \frac{\pi}{3}\nu_A(\rho) = m(\rho)[\pi - \theta(\rho)] - 2\pi, \qquad (4.7)$$

where $\theta(\rho)$ is the included angle in a triple junction, $\pi - \theta(\rho)$ the external rotation angle associated to each side, and the last term 2π compensates the balance for a complete revolution around the grain boundary. It is clear that, in equilibrium conditions, θ does not depend on ρ and it is identically equal to $2\pi/3$. Therefore Eq. (4.7) is identical to Eq. (4.2):

$$\nu_A^\star(\rho) = \frac{\pi}{3}[m(\rho) - 6]. \qquad (4.8)$$

On the contrary, if both $\nu_A^\star(\rho)$ and $m(\rho)$ are known, it can be used to evaluate the angle $\theta(\rho)$ as a function of the reduced grain size:

$$\theta(\rho) = \pi - \frac{2\pi - (\pi/3)\nu_A^\star(\rho)}{m(\rho)}. \qquad (4.9)$$

The deviation from equilibrium for the local curvature model, expressed as $\theta(\rho) - 120°$, is shown in Fig. 8. It is clearly seen that for more than 80% of grains the departure from the equilibrium value is limited within $\pm 2.5°$ and that the standard deviation of such departure on the whole range of topological classes $m(\rho)$ is about 3.6°. As further test, the weighted average of the internal joint angle has been recalculated by the equation

$$\langle \theta \rangle = \sum_{i=1}^{n_c} n_i m_i \theta_i \Big/ \sum_{i=1}^{n_c} n_i m_i \qquad (4.10)$$

which confirmed the value $\langle \theta \rangle = 120°$ expected on the basis of $\langle m \rangle = 6$. This result, which will be further discussed in the following experimental section, is not acceptable if referred to systems where the mechanical equilibrium at triple junctions is surely attained (e.g., soap froths), but it can be plausible for polycrystalline systems.

In soap froths, each cell (grain) contains a fixed volume of gas and molecules permeate through the cell membranes to equalize pressures in adjacent bubbles. The soap froth tends to remain in quasiequilibrium at all times because the cell walls and enclosed gas can adjust almost instantaneously to minimize surface area (i.e., the gas has zero shear modulus and the characteristic time scale for bubble coarsening is greater than that for equilibration of triple joints). As a matter of fact, most of the liquid of the foam is contained at the junctions where the walls are slightly thickened to form the so-called plateau borders. It has been shown that, even in froths, high volume fractions of plateau borders can induce deviations in the angles at triple joints.[34] Therefore it is reasonable to expect that triple junctions in polycrystalline aggregates could be not exactly in equilibrium conditions at a given time because diffusion processes to attain the rearrangement of the boundary network in solids are slow in comparison with those in a gas/liquid soap froth system.[35]

C. Comparison with experiments

The comparison with experiments has been limited to the ability of the model to predict the GSD shape, its kinetic features being in substantial agreement with similar theories. Unfortunately, very few data are available in the literature on normal grain growth in thin films where attention is paid also to the determination of GSD's. Two examples are reported here.

In the first one, GSD's were measured on a 0.5-mm thin sheet of nonoriented 3% Si electrical steel of the following chemical composition (mass %): 0.0050 C, 3.15 Si, 0.21 Mn, 0.0035 N, 0.77 Al, 0.0035 Ti.[36] After cold deformation the sheets were recrystallized and decarburized in hydrogen atmosphere for 180 s at 850 °C (dew point = 35 °C) reducing the carbon content to 0.0020 mass %. Then, four samples were annealed for 60 s at 850, 950, 1050, and 1150 °C, respectively, to activate grain growth. The area of about 1000 grains in each sample was measured by automatic image analysis from optical micrographs of the polished and chemically etched surfaces of the sheets and the data were processed to obtain the distributions of the equivalent radius. The average grain radius and the variation coefficient of the GSD are reported in Table II. Although the average size increases with increasing temperature, the shape of the reduced distribution remains substantially constant, indicating that

TABLE II. Average grain size and variation coefficient of the experimental GSD's measured on 0.5-mm thin sheets of a nonoriented 3% Si electrical steel annealed for 60 s at different temperatures.

Annealing temperature (°C)	$\langle R \rangle$ (μm)	k_{GSD}
850	46.6	0.594
950	79.8	0.590
1050	133.1	0.567
1150	227.3	0.506

normal grain growth occurred. In addition, especially in the sample annealed at 1150 °C, the final grain diameter is almost equal to the sheet thickness.

The reduced GSD's are compared with the theoretical distribution without inhibition in Fig. 9. Again it is worth noting that all the experimental distributions overlap each other and the model fits very well to the data.

In the second example, GSD's measured from a polycrystalline texture-free 80-nm thin film of pure aluminum (99.999%) produced by vacuum evaporation at low temperature on a (100) NaCl substrate[37] have been considered. Grain growth was induced by annealing in a vacuum furnace at 200 °C up to 480 s obtaining average grain sizes ranging from about 30 nm to about 40 nm. Grain-size distributions were determined by measuring the grain area by transmission electron microscopy on more than 500 grains.

The occurrence of normal grain growth was confirmed by a linear relationship between the mean grain area and the annealing time, and by the monomodal GSD's. The size distributions, when plotted as a function of the reduced radius ρ, overlap perfectly, indicating a stationary growth regime with a self-similar GSD shape.

In Fig. 10 the comparison between the experimental distribution determined after the longest annealing time (480 s) and that calculated by the present model with a constant inhibition of 25 mm^{-1} is shown. It can be observed that, although it is necessary to consider a limited inhibition contribution, probably due to the presence of a substrate or to grain-boundary grooving, there is a very good match between the distributions.

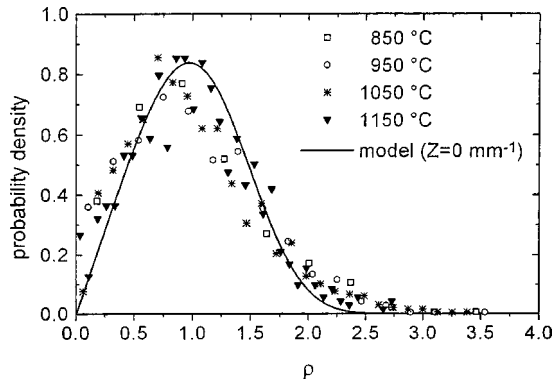

FIG. 9. Comparison among the 2D GSD's measured in a nonoriented 3% Si electrical steel annealed for 60 s at different temperatures (points) and the present model (solid curve).

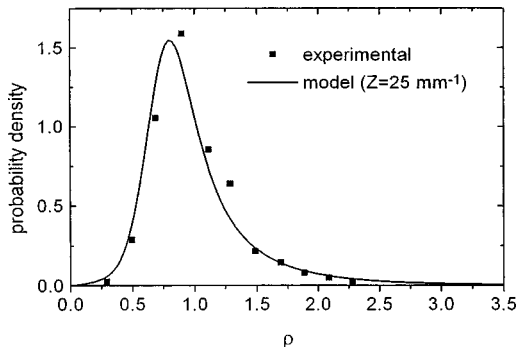

FIG. 10. Comparison between the experimental GSD from Ref. 37 (points) and the quasistationary GSD calculated with 25 mm^{-1} constant inhibition (solid curve).

Finally, in Fig. 11, the model predictions for the von Neumann–Mullins relationship have been compared with the data obtained in experiments on normal 2D grain growth of a 30-mm high, 80-mm long, and 15-mm thin film of succinonitrile (SCN) in controlled conditions,[38] and further reviewed to eliminate the contributions of grains with anomalous behavior.[39] SCN is a low melting point (58.08 °C), easily purified transparent organic material with isotropic properties, often used in solidification studies as a model analog of metals. It permits *in situ* topological measurements as well as the determination of the process kinetics by analyzing the time evolution of the system.

In the experiments, the area growth rate constant for the average grain was determined at a temperature 0.35 °C below the melting temperature of SCN confirming that the process was governed by a parabolic law $\langle \Sigma \rangle \propto t$, or $\langle R \rangle^2 \propto t$. From the analysis of the growth rate of individual grains as a function of their topological class (number of faces), the experimental von Neumann–Mullins diagram was determined with the associated scatter (± 1 standard deviation).

It can be deduced that, although the presence of surface grooving and of the glass surfaces containing the polycrystalline SCN could have affected the system behavior inducing some deviations from ideality, nevertheless the off-equilibrium vNM curve from the local curvature approach

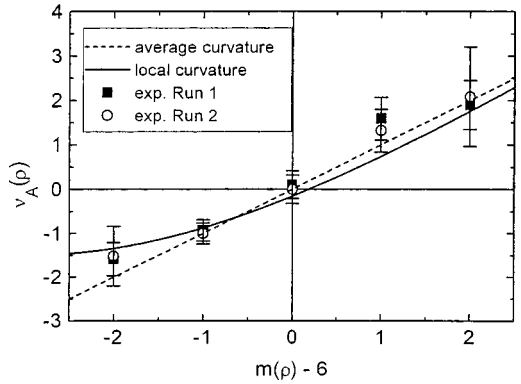

FIG. 11. Von Neumann–Mullins plot of experimental data from 2D grain growth of succinonitrile (points) and comparison with the present model with different descriptions of boundary curvature (curves).

here proposed is not incompatible with the experimental data. On the other hand, the measurement of angles at the triple joints is a very difficult experimental task and deviations of $\pm 2.5°$ from the equilibrium value can be hardly revealed.

No quantitative data are reported to support the hypothesis that this result is also associated with a better description of the GSD shape by the discrete model but the GSD was found to have a right-skewed shape similar to the gamma distribution.[40]

V. CONCLUSIONS

The model, which extends previous analytical theories, predicts the grain growth kinetics and the evolution of the grain-size distribution of a polycrystalline thin film through a probabilistic approach based on elementary interactions between grain pairs together with a simple topological model. The introduction of the local grain-boundary curvature, in contrast with all the analytical 2D models of grain growth in the literature, permits us to obtain a right-skewed asymptotic GSD also in absence of inhibition. Its realistic shape represents a better approximation of the experimental evidences than that of the analytical model by Hillert and similar, where the average boundary curvature is used to evaluate the driving force for grain coarsening. At the same time, it closely approaches the results obtained by numerical models such as Monte Carlo and Surface Evolver.

The effect of inhibition, both constant and time dependent, can be taken into account. A constant inhibition produces a more peaked GSD whose shape resembles a lognormal distribution.

Comparisons with available experimental data show that the model predicts the shape of the GSD of real systems with good accuracy. It is also observed that the introduction of the local grain-boundary curvature causes a slight deviation from linearity in the von Neumann–Mullins plot which is still compatible with the available experimental data. This behavior has been justified admitting a small departure of the average angles at triple junctions from the equilibrium value 120° induced by the local curvature. Therefore the model can be considered for specific applications to polycrystalline solids only where limited off-equilibrium conditions at the junctions can be permitted by the slowness of diffusion processes operating to attain the rearrangement of the boundary network.

*Electronic address: p.dinunzio@c-s-m.it

[1] M. Hillert, Acta Metall. **13**, 227 (1965).
[2] M. P. Anderson, D. J. Srolovitz, G. S. Grest, and P. S. Sahni, Acta Metall. **32**, 783 (1984).
[3] D. J. Srolovitz, M. P. Anderson, P. S. Sahni, and G. S. Grest, Acta Metall. **32**, 793 (1984).
[4] D. J. Srolovitz, M. P. Anderson, G. S. Grest, and P. S. Sahni, Acta Metall. **32**, 1429 (1984).
[5] T. O. Saetre, O. Hunderi, and N. Ryum, Acta Metall. **37**, 1381 (1989).
[6] H. J. Frost, C. V. Thompson, and D. T. Walton, Acta Metall. Mater. **38**, 1455 (1990).
[7] G. Abbruzzese, I. Heckelmann, and K. Lücke, Acta Metall. Mater. **40**, 519 (1992).
[8] K. Lücke, I. Heckelmann, and G. Abbruzzese, Acta Metall. Mater. **40**, 533 (1992).
[9] C. V. Thompson and R. Carel, Mater. Sci. Forum **204–206**, 83 (1992).
[10] K. Marthinsen, O. Hunderi, and N. Ryum, Acta Mater. **44**, 1681 (1996).
[11] J. Geiger, A. Roósz, and P. Barkóczy, Acta Mater. **49**, 623 (2001).
[12] Y. Estrin, G. Gottstein, E. Rabkin, and L. S. Shvindlerman, Acta Mater. **49**, 673 (2001).
[13] S. Sista and T. DebRoy, Metall. Mater. Trans. B **32B**, 1195 (2001).
[14] P. E. Di Nunzio, Acta Mater. **49**, 3635 (2001).
[15] P. E. Di Nunzio, Metall. Mater. Trans. A **33A**, 3329 (2002).
[16] G. Abbruzzese, Acta Metall. **33**, 1329 (1985).
[17] G. Abbruzzese and K. Lücke, Acta Metall. **34**, 905 (1986).
[18] T. Gladman, Proc. R. Soc. London, Ser. A **249A**, 289 (1966).
[19] A. Miyake, Scr. Mater. **45**, 1009 (2001).
[20] W. W. Mullins, Acta Metall. **6**, 414 (1958).
[21] R. Trivedi, in *Lectures on the Theory of Phase Transformations*, edited by H. I. Aaronson (The Metallurgical Society of AIME, New York, 1975), pp. 51–81, Appendix 2, p. 78.
[22] N. P. Louat, Acta Metall. **22**, 721 (1974).
[23] N. P. Louat, M. S. Duesbery, and K. Sadananda, Mater. Sci. Forum **204–206**, 67 (1992).
[24] N. Rivier, Philos. Mag. B **52**, 795 (1985).
[25] E. Carnal and A. Mocellin, Acta Metall. **29**, 135 (1981).
[26] S. K. Kurtz and F. M. A. Carpay, J. Appl. Phys. **51**, 5725 (1980).
[27] S. K. Kurtz and F. M. A. Carpay, J. Appl. Phys. **51**, 5745 (1980).
[28] F. C. Hull, Mater. Sci. Technol. **4**, 778 (1988).
[29] J. von Neumann, *Metal Interfaces* (American Society for Metals, Cleveland, OH, 1952), p. 108.
[30] W. W. Mullins, J. Appl. Phys. **27**, 900 (1956).
[31] N. Rivier, Philos. Mag. B **47**, L45 (1983).
[32] G. Gottstein and L. S. Shvindlerman, Scr. Mater. **38**, 1541 (1998).
[33] G. Gottstein and L. S. Shvindlerman, Scr. Mater. **39**, 1489 (1998).
[34] F. Bolton and D. Weaire, Philos. Mag. B **63**, 795 (1991).
[35] H. V. Atkinson, Acta Mater. **36**, 469 (1988).
[36] A. Campopiano and S. Matera, ECSC Final Report EUR 16700 IT (Contract No. 7210-MA/426), 1997.
[37] S. Protasova and V. Sursaeva, in *Proceedings of the 1st Joint International Conference on Recrystallization and Grain Growth*, edited by G. Gottstein and D. A. Molodov (Springer-Verlag, Berlin, 2001), p. 557.
[38] M. Palmer, K. Rajan, M. E. Glicksman, V. Fradkov, and J. Nordberg, Metall. Mater. Trans. A **26A**, 1061 (1995).
[39] M. A. Palmer, M. E. Glicksman, and K. Rajan, Acta Mater. **46**, 6397 (1998).
[40] K. Rajan (private communication).